DC-Current Injection With Minimum Torque Ripple in Interior Permanent-Magnet Synchronous Motors

Fernando Baneira, Jesús Doval-Gandoy, *Member, IEEE*, Alejandro G. Yepes, *Senior Member, IEEE*, and Oscar López, *Senior Member, IEEE*

***Abstract*—Several proposals based on dc-current injection have been reported for estimating the stator winding resistance in induction machines, and recently extended for synchronous machines. Tracking this resistance can be very useful, e.g., for thermal monitoring or preserving control dynamics. In surface-mounted permanent-magnet synchronous machines (PMSMs), it is possible to inject a dc component in the d-axis, without perturbing the torque. However, it has been claimed that, for synchronous machines with saliency, it is not possible to avoid the torque ripple due to such injection. This letter proposes optimum reference currents to impose dc current in three-phase interior PMSMs while minimizing to practically zero its associated torque ripple. Namely, the dc-signal is injected in combination with a suitable second-order harmonic so that the stator current space vector follows the constant-torque locus, while the fundamental is set according to the maximum-torque-per-ampere strategy. Experimental results validate the theory.**

***Index Terms*—Motor drives, permanent-magnet synchronous machines (PMSMs), signal injection, stator winding resistance.**

I. Introduction

Extensive research has been carried out concerning dc-signal injection for three-phase machines, with the aim of estimating the stator winding resistance [1]–[9]. The updated value of this resistance can be very useful in practice, e.g., to monitor the stator winding temperature (to avoid/detect faults) [1]–[9] or to preserve control dynamics, particularly when it relies on sensorless speed/position estimation [5]–[7].

The underlying principle of these methods is to impose a dc current in the phases, so that a dc voltage drop arises. By extracting the dc current and dc voltage, the stator winding resistance can be obtained [2]. These algorithms are robust to motor parameter variations [9], [10]. However, their main drawback for three-phase induction machines (IMs) is the production of torque ripple [2], [4], [5]. Consequently, in three-phase IMs, a trade-off is made between the magnitude of such ripple and the estimation accuracy [2], [3]. An improved method is proposed in [3] for IMs, based on adding a second-order harmonic to mitigate the torque ripple due to the dc signal. However, smooth torque is not completely attained, due to simplifications in the relatively involved IM model [3].

Recently, these techniques for estimation of stator winding resistance, specifically proposed for three-phase IMs in their origins, have been directly applied to synchronous machines [6]–[8]. For surface-mounted permanent-magnet synchronous machines (SPMSMs), the dc signal is injected in the d-axis (not involved in the torque production), and thus, no extra torque ripple is produced [6], [8]. Nonetheless, it was claimed in [6] that the generation of torque ripple is unavoidable in case of dc-signal injection applied to interior permanent-magnet synchronous machines (IPMSMs), due to reluctance torque.

This letter proposes optimum reference currents with dc-signal injection in three-phase IPMSMs that minimize (to practically zero) the torque ripple generated due to such injection. For this purpose, the reference currents are set so that they follow the constant-torque locus, while the fundamental component complies with the maximum-torque-per-ampere (MTPA) criterion.

II. Review of IPMSM Model and MTPA Strategy

A. IPMSM Model

The model of an IPMSM with sinusoidally distributed windings in a d-q synchronous reference frame is [11]

$$\begin{aligned} v_d &= R_\mathrm{s} i_d + L_d \frac{di_d}{dt} - \omega_\mathrm{e} L_q i_q \\ v_q &= R_\mathrm{s} i_q + L_q \frac{di_q}{dt} + \omega_\mathrm{e} \left(L_d i_d + \lambda_\mathrm{f} \right) \end{aligned} \tag{1}$$

where v and i stand for voltage and current, respectively, R_s is the stator winding resistance, L_d and L_q are the stator self-inductances, ω_e is the electrical rotor angular speed, and λ_f is the permanent-magnet flux linkage (normalized by ω_e). The d-q frame rotates at ω_e so that its d-axis is aligned with λ_f, as usually done for field-oriented control.

The electromagnetic torque T_em can be expressed as [11]

$$T_\mathrm{em} = \frac{3}{2} P \Big[\lambda_\mathrm{f} i_q + \left(L_d - L_q \right) i_d i_q \Big] \tag{2}$$

where P is the number of pole pairs.

Compared with an SPMSM, the distinct characteristic of an IPMSM is the inductance saliency [12]; i.e., L_d is lower than L_q. Note that in (2) there are two addends. The first one, called mutual torque, is produced by the interaction of i_q and the permanent-magnet flux. The second addend is the reluctance torque, which is caused by the saliency. For an SPMSM ($L_d = L_q$), the reluctance torque in (2) is zero.

Manuscript received May 7, 2019; revised June 6, 2019 and July 20, 2019; accepted July 27, 2019. Date of publication XXXX; date of current version XXXX. This work was supported by the Spanish Ministry of Science and Innovation and by the European Commission, European Regional Development Fund (ERDF) under project DPI2016-75832.

F. Baneira, J. Doval-Gandoy, A. G. Yepes and O. López are with the Applied Power Electronics Technology (APET) Research Group, University of Vigo, Vigo 36310, Spain (e-mail: fbaneira@uvigo.es; jdoval@uvigo.es; agyepes@uvigo.es; olopez@uvigo.es).

Color versions of one or more of the figures in this paper are available online at http://ieeexplore.ieee.org.

Digital Object Identifier XXXX

B. MTPA Strategy

Usually, the reference currents in the d-q frame (corresponding to fundamental current in stationary coordinates) are

$$i_{d1} = I_1 \cos(\phi_1), \qquad i_{q1} = I_1 \sin(\phi_1) \tag{3}$$

where ϕ_1 is the angle between the fundamental current space vector (SV) $\underline{i}_1 = i_{d1} + j i_{q1}$ and the d-axis, and I_1 is the magnitude of $\underline{i}_1$. Among all ϕ_1 values, the one that yields maximum torque for given I_1 is [11]–[13]

$$\phi_{\text{MTPA}} = \cos^{-1}\left(\frac{-\lambda_{\text{f}} + \sqrt{\lambda_{\text{f}}^2 + 8(L_d - L_q)^2 I_1^2}}{4\,(L_d - L_q)\,I_1}\right) \tag{4}$$

which defines the widely-used [14] MTPA strategy. If (3) is substituted in (2), the differentiation of (2) with respect to ϕ_1 (for certain I_1) $\partial T_{\text{em}}/\partial\phi_1$ is zero when evaluated at the MTPA point ($\phi_1 = \phi_{\text{MTPA}}$). The MTPA and constant-torque loci are depicted in Fig. 1(a). The SV of the total stator current $\underline{i}_{\text{s}}$ (with phase angle ϕ) equals $\underline{i}_1$, because only fundamental is considered so far. As can be observed, for given torque reference $T_{\text{em}}^{\text{ref}}$, the $\underline{i}_{\text{s}}$ SV is fixed at a point in the d-q frame, with positive i_q and negative i_d (for motor mode).

III. Reference Currents for DC Injection

A. Conventional Method

In general, dc currents can be injected in the three-phase windings of IPMSMs controlled by field-oriented control by superimposing on the fundamental current reference a dc component in the α-β frame, as done in [2], [5] for IMs:

$$\Delta i_\alpha = I_{\text{dc}}, \qquad \Delta i_\beta = 0 \tag{5}$$

or expressed in the d-q frame:

$$\Delta i_d = I_{\text{dc}} \cos(\theta_{\text{e}}), \qquad \Delta i_q = -I_{\text{dc}} \sin(\theta_{\text{e}}) \tag{6}$$

where I_{dc} is the magnitude of the injected dc-current reference, and θ_{e} is the electric rotor position.

Fig. 1(b) depicts the trajectory described by the stator current SV in the d-q frame for given $T_{\text{em}}^{\text{ref}}$ while injecting dc current [as (5)] in IPMSMs. In this figure, the SV $\underline{i}_{\text{s}}$ is composed of two SVs; one for the injected currents according to (5) $\underline{i}_{\text{dc}}^{\text{conv}}$, and the fundamental SV $\underline{i}_1$, which satisfies the MTPA condition (4). The superscript conv stands for conventional method. As can be observed, the $\underline{i}_{\text{s}}$ trajectory in this case is not fixed at a point anymore, as in Fig. 1(a), but is instead a circumference of radius I_{dc}. This SV in the d-q frame rotates in counter-clockwise direction at the electric rotor speed. Such current injection produces extra torque ripple [2], [6], as can also be inferred from Fig. 1(b).

B. Proposed Optimum Reference Currents

As depicted in Fig. 1, the constant-torque locus (its tangent) is perpendicular to $\underline{i}_1$, when the latter is set according to the MTPA strategy. This stems from the fact that, as aforesaid, $\partial T_{\text{em}}/\partial\phi_1$ is zero at $\phi_1 = \phi_{\text{MTPA}}$. In order not to disturb T_{em}, the optimum injected current $\underline{i}_{\text{dc}}^{\text{opt}}$ must move approximately along this constant-torque line, as illustrated in Fig. 1(c). In general, an SV trajectory in the d-q plane along a straight line

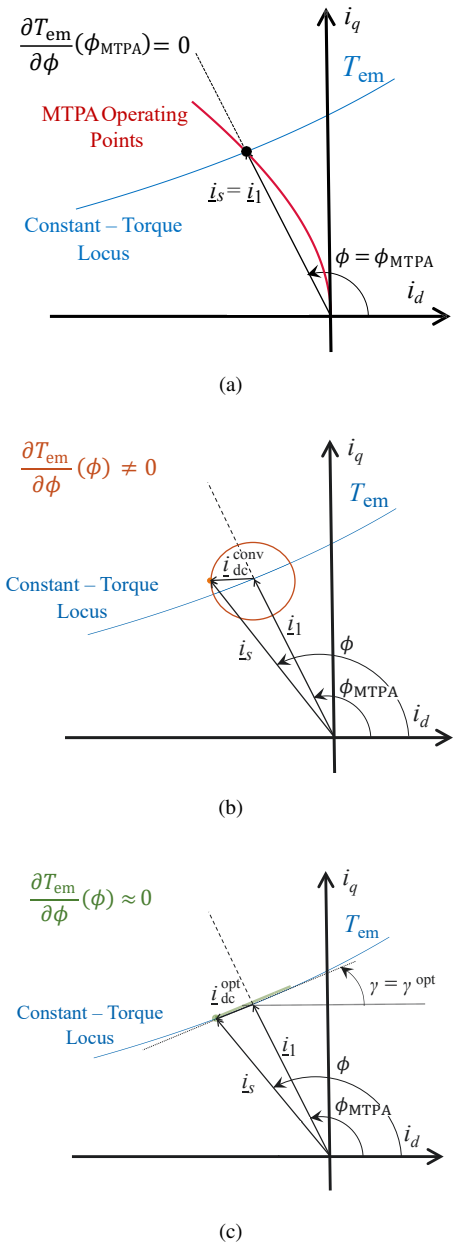

Fig. 1. Trajectory described by the SV $\underline{i}_{\text{s}}$ in the d-q frame for a given $T_{\text{em}}^{\text{ref}}$, where the fundamental component $\underline{i}_1$ is selected according to the MTPA strategy, i.e., (4). (a) No injection ($\underline{i}_{\text{s}}$ is fixed at a point). (b) Conventional dc injection according to (5) ($\underline{i}_{\text{s}}$ describes a circumference). (c) Optimized dc injection according to (12) ($\underline{i}_{\text{s}}$ describes a straight line).

forming an angle γ with the d-axis is given in complex-vector notation by

$$\Delta \underline{i}_{dq} = I_{\text{dc}} \left[\text{e}^{-j\theta_{\text{e}}} + \text{e}^{j(\theta_{\text{e}}+2\gamma)}\right] \tag{7}$$

or in scalar notation (using trigonometric identities[1]) by

$$\begin{aligned} \Delta i_d &= \mathfrak{Re}\left\{\Delta \underline{i}_{dq}\right\} = 2 I_{\text{dc}} \cos(\gamma)\cos(\theta_{\text{e}} + \gamma) \\ \Delta i_q &= \mathfrak{Im}\left\{\Delta \underline{i}_{dq}\right\} = 2 I_{\text{dc}} \sin(\gamma)\cos(\theta_{\text{e}} + \gamma). \end{aligned} \tag{8}$$

[1]Note that $2\cos(\varphi)\cos(\delta) = \cos(\varphi+\delta) + \cos(\varphi-\delta)$ and $2\sin(\varphi)\cos(\delta) = \sin(\varphi+\delta) + \sin(\varphi-\delta)$.

Equation (7) can be understood as the addition of two SVs rotating at ω_e in opposite directions. The SV components that are perpendicular to such straight line of angle γ are always canceled with each other. The magnitude of (7) is maximum when both addends are equal, i.e., when $\Delta\underline{i}_{dq} = 2I_{dc}e^{j\gamma}$, whose phase angle is obviously γ. It can also be noted from (8) that $\arctan(\Delta i_q/\Delta i_d)$ is always γ. Substitution of $\gamma = 0$ in (7) and (8) would result in the well-known case of a real-valued cosine signal. One of the two γ options

$$\gamma^{\text{opt}} = \phi_{\text{MTPA}} \pm \frac{\pi}{2} \tag{9}$$

should be set to ensure that the total SV follows the constant-torque locus (approximated by a straight line perpendicular to $\underline{i}_1$) once Δi_{dq} is added to the fundamental references in (3):

$$i_d = i_{d1} + \Delta i_d, \qquad i_q = i_{q1} + \Delta i_q. \tag{10}$$

The signals in (7) and (8) may be transformed to the stationary α-β frame by multiplying by $e^{j\theta}$, which results in

$$\Delta\underline{i}_{\alpha\beta} = I_{dc}\left[1 + e^{j(2\theta_e+2\gamma)}\right] \tag{11}$$

or equivalently

$$\begin{aligned}\Delta i_\alpha &= \mathfrak{Re}\left\{\Delta\underline{i}_{\alpha\beta}\right\} = I_{dc} + I_{dc}\cos(2\theta_e + 2\gamma)\\ \Delta i_\beta &= \mathfrak{Im}\left\{\Delta\underline{i}_{\alpha\beta}\right\} = I_{dc}\sin(2\theta_e + 2\gamma).\end{aligned} \tag{12}$$

Therefore, to minimize torque ripple, the injected current, when expressed in stationary frame, should include a second-order harmonic with initial phase 2γ in addition to the dc offset. This is the novel approach proposed in this letter.

In [3], a second-order component is also injected in IMs; however, in [3] γ is chosen to be zero. For IPMSMs, the selection of γ according to (9) is crucial for good torque ripple minimization, which is the main contribution of this letter.

Note that, if I_{dc} were excessively large, the $\underline{i}_s$ trajectory could not be assumed to follow the constant-torque locus, and thus, some non-negligible extra torque ripple would arise.

It should be emphasized that the only dependency of (7)-(12) on machine parameters occurs through ϕ_{MTPA} in (9), since ϕ_{MTPA} is related to parameters such as L_d and L_q [see (4)]. Adaptive MTPA methods [11]–[13] can be adopted to modify ϕ_{MTPA} online under parameter variations (e.g., associated to temperature or saturation). With such adjustment, it is still ensured that $\partial T_{em}/\partial\phi_1$ is zero at ϕ_{MTPA}, and consequently, that the proposed references provide minimum torque ripple.

The effect of core loss on the optimum fundamental current [and hence, on (7)-(12)] can be neglected in the base-speed region [11]–[13], as done in MTPA techniques. Otherwise, if losses other than stator copper loss are deemed important (e.g., in the field-weakening region), strategies more advanced than MTPA could be adopted to set the fundamental component for better efficiency [14], [15], at the cost of substantial increase in complexity. Modification of (7)-(12) for minimum torque ripple in such case may be the subject of future work.

Concerning implementation, the proposal can be put into practice by computing (12) in α-β frame or (8) in d-q frame.

TABLE I
PARAMETERS OF THREE-PHASE IPMSM

Parameter	Symbol	Value
Rated power	P_r	3356 W
Rated current	I_r	8.84 A
Rated speed	n_r	2500 r/min
Pole pairs	P	3
Stator resistance at 20°C	R_s	0.1778 Ω
Inductance in the d-axis	L_d	5.026 mH
Inductance in the q-axis	L_q	10.23 mH
Stator leakage inductance	L_{ls}	0.348 mH
Voltage constant (line rms)	λ_f	0.082 V/r/min

The latter allows fewer operations, taking into account that

$$\cos\left(\gamma^{\text{opt}}\right) = -\sin\left(\phi_{\text{MTPA}}\right), \qquad \sin\left(\gamma^{\text{opt}}\right) = \cos\left(\phi_{\text{MTPA}}\right) \tag{13}$$

holds [considering + in (9)], and that these two terms in (13) already need to be calculated for the fundamental component [see (3)]. Moreover, the expression $2I_{dc}\cos(\theta_e+\gamma^{\text{opt}})$, included in both parts of (8), only requires to be evaluated once, and using (13) it can be further simplified as

$$\begin{aligned}2I_{dc}\cos\left(\theta_e + \gamma^{\text{opt}}\right) = -2I_{dc}\left[\cos\left(\theta_e\right)\sin\left(\phi_{\text{MTPA}}\right)\right.\\ \left.+\sin\left(\theta_e\right)\cos(\phi_{\text{MTPA}})\right]\end{aligned} \tag{14}$$

where $\cos(\theta_e)$ and $\sin(\theta_e)$ are normally already calculated for the frame (Park) transformations. As a consequence, (8) can be computed in real time by adding only six multiplications and one addition to the rest of the operations. Then, just two extra additions should be applied to include the resulting Δi_d and Δi_q in the total current references [see (10)]. Therefore, the computational load of the proposal is negligible for modern microprocessors and digital signal processors.

IV. EXPERIMENTAL RESULTS

An IPMSM with the parameters displayed in Table I is employed for the experimental tests. The SEMIKRON three-phase converter used to drive this machine is based on insulated-gate bipolar transistors. The digital control is run in a dSPACE-DS1006 platform, including the AC Motor Control Solution in an expansion box. The DS1006 Processor Board is based on a quad-core AMD Opteron x86 processor with 2.8-GHz clock frequency. Matlab/Simulink environment is employed to implement the drive control and compile it to C-program, which is then built to the dSPACE-compatible real-time program [16]. ControlDesk software is used as a graphical interface with the dSPACE platform during the tests. The sampling and switching frequencies are set to 10 kHz. In accordance with Section II, the torque reference for the IPMSM is imposed in closed-loop by means of conventional field-oriented control with MTPA strategy. Besides the proportional-integral current controller in the d-q frame rotating at ω_e, additional integral parts [9] are also included to track the dc and second-order components in (12). The fundamental control gains are tuned as a function of the nominal system parameters as in [17], the gains of the additional integral parts are set

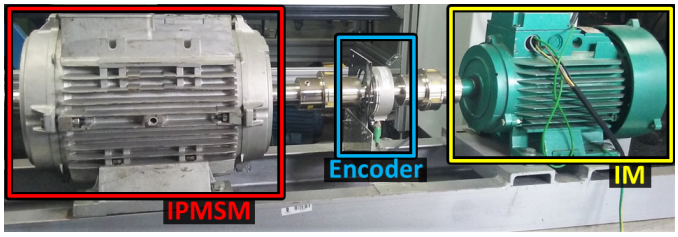

Fig. 2. Picture of the experimental test bench.

to 20% of the fundamental ones, and an active resistance is introduced [17] to improve the disturbance rejection. The rotor position is measured by an encoder (see Fig. 2).

As shown in Fig. 2, the IPMSM is mechanically coupled with an IM. The latter is fed by an adjustable speed drive, which works in speed-control mode. In the tests, the IPMSM runs at $n = 500\,\mathrm{r/min}$. Given that ω_e is absent in (2), the effect of dc current on the magnitude of the torque ripple is not expected to vary with the average speed. Regarding speed ripple, operation at relatively low ω_e (as $500\,\mathrm{r/min}$) is more critical, since the amplitude of the speed oscillations is then larger compared with its average [9], [18].

When (12) is used to inject the dc component during the tests, (9) is also applied, unless the contrary is explicitly mentioned.

Once the dc signal is injected into the phase windings, any of the algorithms presented in [2], [3], [10] can be used to extract the dc components from the phase voltages and currents, and subsequently, estimate the stator winding resistance. Hence, experimental tests similar to the ones presented in [2], [3], [10] regarding the estimation of stator winding resistance are not repeated here. It is worth to remark that the contribution of this letter is the optimization of the reference currents for torque ripple minimization, and not a method to estimate the stator winding resistance from the measurements.

A. Influence of DC-Signal Injection on the Phase Currents

In this section, the phase currents and their spectrum, using (5) and (12), are discussed.

First, a dc signal is injected by using the conventional approach (5). The magnitude of the injected signal is $I_{dc} = 1\,\mathrm{A}$, which is 13.3% of the fundamental current peak $I_1 = 7.5\,\mathrm{A}$. This dc current has been selected to be very large on purpose, only for this experiment, so as to be able to visually verify its influence on the phase currents, which are shown in Fig. 3(a). As expected, an offset (due to the injection) can be observed in one phase with respect to the other two. Furthermore, the spectrum of the current in phase-a is depicted in Fig. 4. As can be observed in this figure, the signal is composed of a fundamental component and a dc offset.

On the other hand, Fig. 3(b) shows the waveforms of the phase currents when the reference currents according to (12) and (9) are injected. The waveforms in Fig. 3(b) are more distorted than the ones in Fig. 3(a). Fig. 4 also shows the spectrum of phase-a for the optimized injection, where it can be seen that this signal is composed of dc, fundamental and second-order components, as expected from (12).

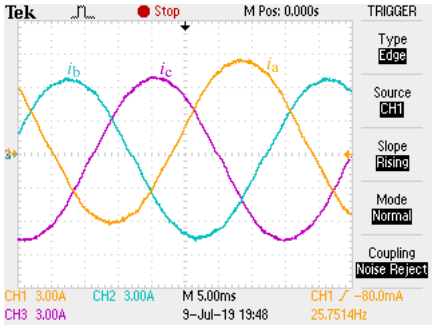

(a)

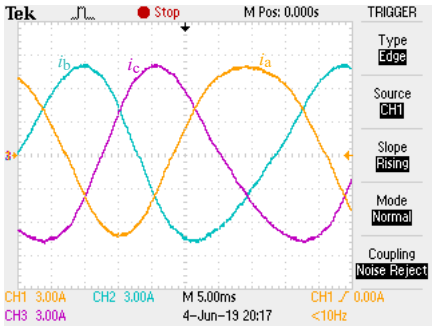

(b)

Fig. 3. Waveforms of the phase currents. (a) Conventional dc injection according to (5). (b) Optimized dc injection according to (12).

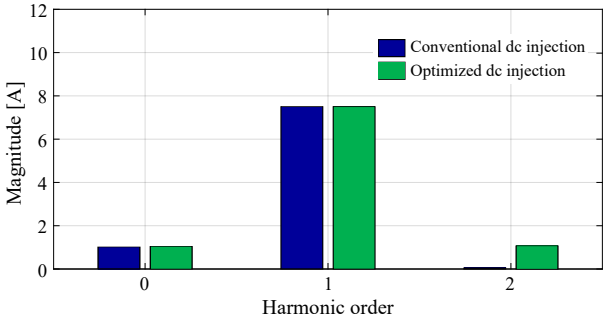

Fig. 4. Spectrum of the phase-a current in the stationary reference frame.

B. Influence of DC Signal on the Torque

Next, the influence of the injected signals on T_{em}, which is estimated by means of (2), as done, e.g., in [10], [19], is shown before and during the injection. According to (5), a dc offset of magnitude $I_{dc} = 0.5\,\mathrm{A}$ ($I_{dc}/I_1 = 6.7\%$) is injected, while the average reference torque T_{em} is $8\,\mathrm{Nm}$. As expected, a ripple at the rotor electrical frequency of 20 Hz is perceived in T_{em} during the dc-signal injection [see Fig. 5(a)], in a manner similar to [2], [6].

The torque produced when the currents according to (12) are injected is also shown in Fig. 5(a). As in the previous case, the injected dc current is 6.7% of the fundamental one. As can be seen in Fig. 5(a), the torque ripple caused by the proposed injected currents is negligible; hence, the machine torque is not affected by the injected signal. This is the most important conclusion to be drawn from this figure.

Fig. 5(b) shows T_{em} before and after the injection, when the magnitude of the injected signals is $I_{dc} = 1\,\mathrm{A}$ (13.3%

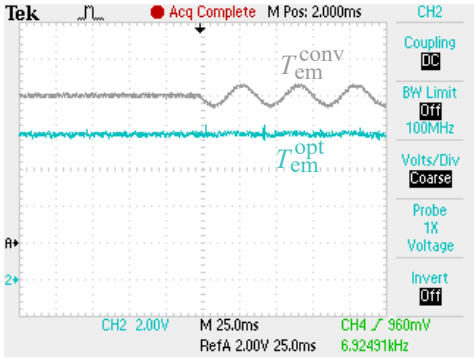

(a)

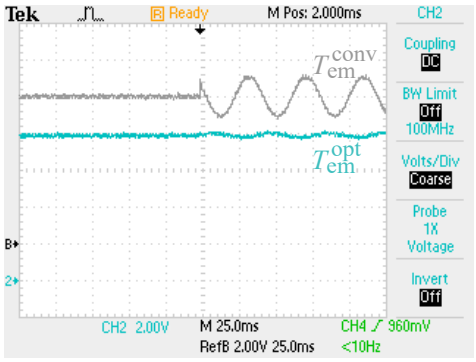

(b)

Fig. 5. Torque T_{em} before and during the conventional (gray) and the optimized (blue) dc injection. T_{em} scale: 2 Nm/div. (a) $I_{\text{dc}}/I_1 = 6.7\%$. (b) $I_{\text{dc}}/I_1 = 13.3\%$.

of I_1). As expected from the theoretical analysis, since I_{dc} is larger, a small torque ripple appears in the optimized approach. Nevertheless, it is highly reduced compared with the conventional case using (5).

C. Influence of the Phase Angle γ on the Torque

The influence of the selection of the phase angle of the second-order harmonic on the torque ripple is assessed in the following. Fig. 6 shows the ripple (theoretical and experimental) in T_{em} as a function of γ. From this figure, it can be clearly observed that the selection of this angle is crucial for a good minimization in the perturbation in T_{em} while injecting a dc signal according to (12). When $\gamma = \gamma^{\text{opt}} \pm \pi/2 = \phi_{\text{MTPA}}$, the torque ripple due to the injection is maximum, being even larger than the one produced due to the conventional approach (5), also shown in Fig. 6 for comparison. On the other hand, as expected, when $\gamma = \gamma^{\text{opt}}$, and $\gamma = \gamma^{\text{opt}} \pm \pi$, the torque ripple is minimum.

D. d-q Current Waveforms

Lastly, the reference and actual d-q current signals for a step in the reference torque from 0 Nm to 8 Nm, with the optimized signal injection, are shown in Fig. 7. The dc current is set to just $I_{\text{dc}} = 0.4$ A so that the dynamic response in the average components of i_d and i_q (corresponding to fundamental in stationary frame) can be more clearly observed. The test of Fig. 7(a) is carried out by setting the system parameters in

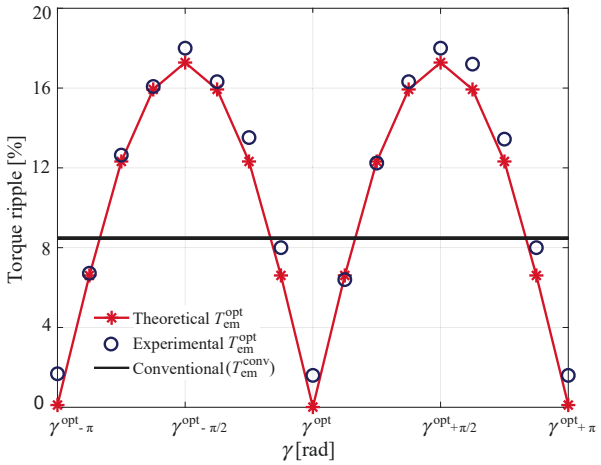

Fig. 6. Magnitude of torque ripple as a function of γ, for $I_{\text{dc}}/I_1 = 5\%$.

the control to their nominal values, whereas in the test of Fig. 7(b) a demanding situation with parameter deviations is emulated. Namely, a $+30\%$ deviation is introduced in R_{s} and L_q, while a -30% deviation is applied to L_d. In both cases, the current waveforms achieve a good tracking of their respective references in a very short time after the change takes place. There is some ripple due to system nonlinearities, but its magnitude is small. In case even larger deviations are expected and robustness is of particular relevance, algorithms to adapt ϕ_{MTPA} [11]–[13] and the machine parameters [20], [21] may be adopted in combination with the proposal.

V. Conclusions

In this letter, optimum current references for dc-signal injection in three-phase IPMSMs are presented. By applying the proposed references, the stator current moves along the constant-torque locus while the fundamental component satisfies the MTPA criterion. In this manner, the torque ripple associated to the dc current is effectively minimized (which was never attained so far in IPMSMs) while saliency is exploited. Experimental results with a three-phase IPMSM verify the functionality of the proposal.

References

[1] P. Zhang, B. Lu, and T. G. Habetler, "A remote and sensorless stator winding resistance estimation method for thermal protection of soft-starter-connected induction machines," *IEEE Trans. Ind. Electron.*, vol. 55, no. 10, pp. 3611–3618, Oct. 2008.

[2] S. Cheng, Y. Du, J. Restrepo, P. Zhang, and T. Habetler, "A nonintrusive thermal monitoring method for induction motors fed by closed-loop inverter drives," *IEEE Trans. Power Electron.*, vol. 27, no. 9, pp. 4122–4131, Sep. 2012.

[3] L. He, J. Restrepo, S. Cheng, R. G. Harley, and T. G. Habetler, "An improved dc-signal-injection method with active torque-ripple mitigation for thermal monitoring of field-oriented-controlled induction motors," in *Proc. IEEE ECCE*, Sep. 2015, pp. 4447–4454.

[4] L. He, S. Cheng, Y. Du, R. G. Harley, and T. G. Habetler, "Stator temperature estimation of direct-torque-controlled induction machines via active flux or torque injection," *IEEE Trans. Power Electron.*, vol. 30, no. 2, pp. 888–899, Feb. 2015.

[5] P. R. Matic, M. A. Gecic, D. M. Lekic, and D. P. Marcetic, "Thermal protection of vector-controlled IM drive based on dc current injection," *IEEE Trans. Ind. Electron.*, vol. 62, no. 4, pp. 2082–2089, Apr. 2015.

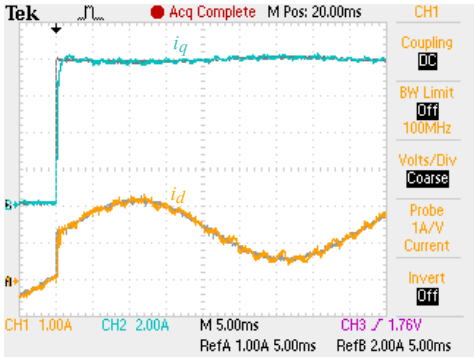

(a)

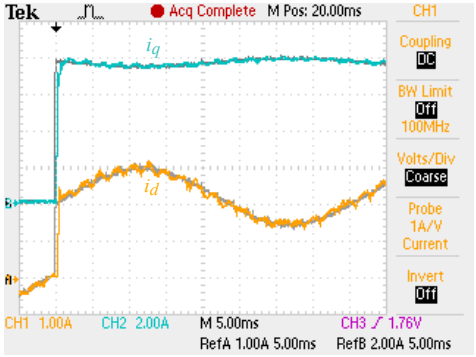

(b)

Fig. 7. d- and q-axis currents (reference and actual currents, in gray and other colors, respectively) during a step in the average $T_{\text{em}}^{\text{ref}}$ from $0\,\text{Nm}$ to $8\,\text{Nm}$, with the optimized signal injection. (a) Without parameter deviations. (b) With parameter deviations.

[6] R. Antonello, L. Ortombina, F. Tinazzi, and M. Zigliotto, "Online stator resistance tracking for reluctance and interior permanent magnet synchronous motors," *IEEE Trans. Ind. Appl.*, vol. 54, no. 4, pp. 3405–3414, Jul./Aug. 2018.

[7] G. Zanuso, L. Peretti, and P. Sandulescu, "Stator reference frame approach for dc injection-based stator resistance estimation in electric drives," in *Proc. IEEE PEDS*, Jun. 2015, pp. 867–872.

[8] S. D. Wilson, P. Stewart, and B. P. Taylor, "Methods of resistance estimation in permanent magnet synchronous motors for real-time thermal management," *IEEE Trans. Energy Convers.*, vol. 25, no. 3, pp. 698–707, Sep. 2010.

[9] F. Baneira, L. Asiminoaei, J. Doval-Gandoy, H. A. M. Delpino, A. G. Yepes, and J. Godbersen, "Estimation method of stator winding resistance for induction motor drives based on dc-signal injection suitable for low inertia," *IEEE Trans. Power Electron.*, vol. 34, no. 6, pp. 5646–5654, Jun. 2019.

[10] F. Baneira, A. G. Yepes, O. Lopez., and J. Doval-Gandoy, "Estimation method of stator winding temperature for dual three-phase machines based on dc-signal injection," *IEEE Trans. Power Electron.*, vol. 31, no. 7, pp. 5141–5148, Jul. 2016.

[11] S. Kim, Y.-D. Yoon, S.-K. Sul, and K. Ide, "Maximum torque per ampere (MTPA) control of an IPM machine based on signal injection considering inductance saturation," *IEEE Trans. Power Electron.*, vol. 28, no. 1, pp. 488–497, Jan. 2013.

[12] C. Lai, G. Feng, K. Mukherjee, J. Tjong, and N. C. Kar, "Maximum torque per ampere control for IPMSM using gradient descent algorithm based on measured speed harmonics," *IEEE Trans. Ind. Informat.*, vol. 14, no. 4, pp. 1424–1435, Apr. 2018.

[13] T. Sun, J. Wang, and X. Chen, "Maximum torque per ampere (MTPA) control for interior permanent magnet synchronous machine drives based on virtual signal injection," *IEEE Trans. Power Electron.*, vol. 30, no. 9, pp. 5036–5045, Sep. 2015.

[14] A. Balamurali, G. Feng, C. Lai, J. Tjong, and N. C. Kar, "Maximum efficiency control of PMSM drives considering system losses using gradient descent algorithm based on dc power measurement," *IEEE Trans. Energy Convers.*, vol. 33, no. 4, pp. 2240–2249, Dec. 2018.

[15] M. N. Uddin, M. M. Rahman, B. Patel, and B. Venkatesh, "Performance of a loss model based nonlinear controller for IPMSM drive incorporating parameter uncertainties," *IEEE Tran. Power Electron.*, vol. 34, no. 6, pp. 5684–5696, Jun. 2019.

[16] A. Gebregergis and P. Pillay, "Implementation of fuel cell emulation on DSP and dSPACE controllers in the design of power electronic converters," *IEEE Trans. Ind. Appl.*, vol. 46, no. 1, pp. 285–294, Jan. 2010.

[17] A. G. Yepes, A. Vidal, J. Malvar, O. Lopez, and J. Doval-Gandoy, "Tuning method aimed at optimized settling time and overshoot for synchronous proportional-integral current control in electric machines," *IEEE Trans. Power Electron.*, vol. 29, no. 6, pp. 3041–3054, Jun. 2014.

[18] A. Houari, A. Bouabdallah, A. Djerioui, M. Machmoum, F. Auger, A. Darkawi, J. Olivier, and M. F. Benkhoris, "An effective compensation technique for speed smoothness at low-speed operation of PMSM drives," *IEEE Trans. Ind. Appl.*, vol. 54, no. 1, pp. 647–655, Jan. 2018.

[19] M. Mengoni, L. Zarri, A. Tani, G. Serra, and D. Casadei, "A comparison of four robust control schemes for field-weakening operation of induction motors," *IEEE Trans. Power Electron.*, vol. 27, no. 1, pp. 307–320, Jan. 2012.

[20] D. Q. Dang, M. S. Rafaq, H. H. Choi, and J. Jung, "Online parameter estimation technique for adaptive control applications of interior PM synchronous motor drives," *IEEE Trans. Ind. Electron.*, vol. 63, no. 3, pp. 1438–144, Mar. 2016.

[21] M. S. Rafaq, F. Mwasilu, J. Kim, H. H. Choi, and J. Jung, "Online parameter identification for model-based sensorless control of interior permanent magnet synchronous machine," *IEEE Trans. Power Electron.*, vol. 32, no. 6, pp. 4631–4643, Jun. 2017.